



# Effect of vacuum annealing on structural and optical properties of nanocrystalline ZnTe thin films

Harinder Singh<sup>1</sup> · Neha Duklan<sup>1</sup> · Tejbir Singh<sup>2</sup> · Anup Thakur<sup>3</sup> · Jeewan Sharma<sup>1</sup>

Received: 16 October 2017 / Accepted: 19 December 2017 / Published online: 26 December 2017  
© Springer Science+Business Media, LLC, part of Springer Nature 2017

## Abstract

In present study, dependence of structural and optical properties of nanocrystalline  $Zn_{40}Te_{60}$  (ZnTe) thin films on vacuum thermal annealing has been investigated. ZnTe alloy was prepared by melt quenching technique and thermally evaporated on cleansed glass substrates to deposit thin films. These films were annealed in vacuum ( $\sim 1 \times 10^{-3}$  mbar) for an hour at three different temperatures 100, 200 and 300 °C. X-ray diffraction results revealed the presence of cubic ZnTe phase in all the films along with some hexagonal Te phase. The crystallite size of ZnTe thin films improved on annealing with larger size at elevated temperatures (from 32 to 80 nm). Micro strain and dislocation density reduced owing to improvement in crystallinity after annealing. The IR transmittance increased with increase in annealing temperature. Field emission scanning electron microscopy images suggested the formation of smooth and uniform thin films with thickness of  $\sim 480$  nm. Optical properties revealed the decrease in transmittance and absorption edge shift due to crystallinity improvement on annealing. The optical band gap decreased from 1.37 to 0.91 eV on annealing. Experimental results show that thermal annealing has significant impact on structural and optical properties of ZnTe thin films.

## 1 Introduction

The ever-growing energy demands is one of the main challenges of twenty-first century. Conventional energy resources i.e. fossil fuels (coal, natural gas and oil) are limited in nature and these are exhausting swiftly. The environmental degradation is associated with power generation through burning of these fossil fuels in form of sulfur dioxide and carbon dioxide gases released during burning process. Developing economical, reliable and environment friendly renewable energy resources is the need of hour [1–3]. Solar energy is one of the preminent substitutes for green energy as it is sustainable and abundant hence, photovoltaics have attracted massive interest in terms of research and development from last few decades [4, 5]. Photovoltaics technologies for solar energy conversion render auspicious

routes to renewable and green energy [6]. Thin film photovoltaics have been employed since 1883 when Charles Fritts fabricated primitive solar cell on a metal foil coated with selenium and thin gold layer. Crystalline silicon based solar cells were developed in 1950s, confronted many challenges such as indirect band gap, multi-step fabrication process, high fabrication cost, requirement of large quantities of ultra-pure material and maximum attainable efficiency upto 33.7% as measured by Shockley and Queisser [3, 7]. From past few decades, significant evolution in variety of thin film solar cells has been achieved, which remarkably lowers the processing cost because of small thickness of an absorber layer [8]. The thin film metal chalcogenide solar cells are found to be cost effective and have shown high efficiency as compare to conventional silicon based photovoltaics [9].

The II-VI family of semiconductors, including zinc selenide (ZnSe), cadmium selenide (CdSe), zinc telluride (ZnTe) and cadmium telluride (CdTe) has attracted considerable attention of scientists and engineers for photovoltaic and photoelectrochemical cells due to high absorption coefficient and low cost [10]. These materials possess other applications such as nonlinear optical detectors, laser screen materials and light emitting diodes, etc. [11, 12]. Due to toxic nature of cadmium and cadmium-based chalcogenides, many research groups are looking to explore less toxic metals, such

✉ Jeewan Sharma  
jeewansharma29@gmail.com

<sup>1</sup> Department of Nanotechnology, Sri Guru Granth Sahib World University, Fatehgarh Sahib 140 407, India

<sup>2</sup> Department of Physics, Sri Guru Granth Sahib World University, Fatehgarh Sahib 140 407, India

<sup>3</sup> Department of Basic and Applied Sciences, Punjabi University, Patiala, Punjab 147 002, India

as zinc chalcogenide specially ZnTe [13]. ZnTe is a p-type semiconducting material with direct band gap reported to vary from 1.7 to 2.6 eV [10, 14], exciton Bohr radius of  $\sim 7$  nm and low affinity (3.53 eV) [13]. ZnTe thin films are used as back contact in CdTe/CdS heterojunction solar cells because of its 0.1 eV offset value and provide better module stability and champion cell efficiency [15, 16]. ZnTe thin films are also used in modern technologies of solid-state devices such as green colour light emitting diodes and photodetectors because of its low resistivity, wide band gap and high transparency in visible spectrum domain [17]. Some other important applications of ZnTe includes micro-wave devices, electroluminescent devices, thermoelectric and optoelectronic devices, electro-optic field detectors, buffer layers for infra-red detectors, light source in television projectors and host candidates for X-ray phosphor screens [13]. ZnTe is outstanding material as a potential candidate for fabrication of heterostructures with quantum-dimensional properties [11].

Literature study reveals that ZnTe thin films can be deposited by various techniques including thermal evaporation [18], electro deposition [19], RF sputtering [20], DC sputtering [15], magnetron sputtering [21], metal organic vapour phase epitaxy (MOVPE) and metal organic chemical vapour deposition (MOCVD) [22], vapor phase epitaxy [23], molecular beam epitaxy [24], electrochemical process [25] and closed space sublimation [26]. Thermal evaporation technique is chosen for thin film preparation due to its many advantages. It provides thin films on large area and gives better control of deposition rate, film thickness and temperature [27]. The thermal annealing is done in vacuum due to its advantage that, specimen will not be oxidized during heat treatment. Some researchers report annealing of  $\text{Zn}_{50}\text{Te}_{50}$  thin films in different ambients like air [28, 29], Ar [18, 30] and  $\text{N}_2$  [31, 32]. It is observed that annealing done in nitrogen ambience is performed for doping purposes [31].

In the present study, the effect of vacuum annealing on nanocrystalline  $\text{Zn}_{40}\text{Te}_{60}$  thin films has been studied. In previous study on different compositions of ZnTe,  $\text{Zn}_{40}\text{Te}_{60}$  had shown almost similar structural properties as  $\text{Zn}_{50}\text{Te}_{50}$  [33]. Hence, an effort has been made to synthesize nanocrystalline  $\text{Zn}_{40}\text{Te}_{60}$  thin films by thermal evaporation and analyze the effect of vacuum annealing on structural and optical properties of these films.

## 2 Experimental

Zinc and tellurium (5N pure) were procured from Sigma-Aldrich, India. To prepare 2g  $\text{Zn}_{40}\text{Te}_{60}$  alloy sample, zinc and tellurium elements were weighed 0.050922 and 1.49077 g, respectively using electronic balance (Mettler TOLEDO, ML204/A01). These elements were sealed in a quartz

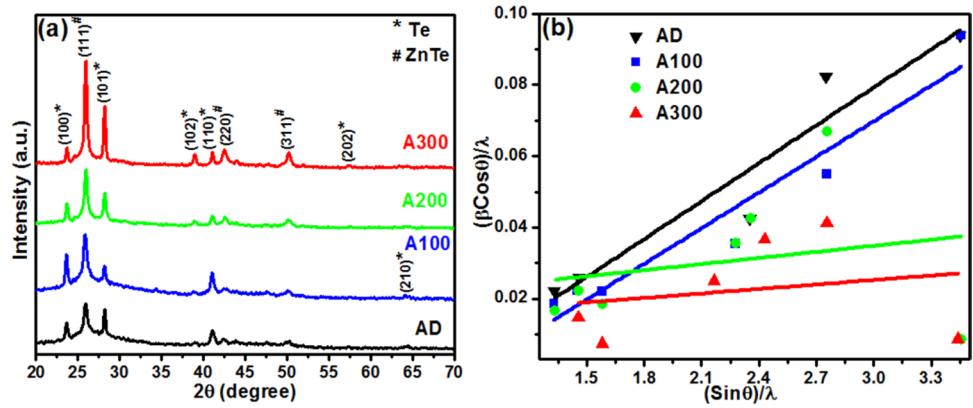
ampoule with  $\sim 8$  mm internal diameter and kept in muffle furnace (Lenton, UAF14/10) for 23 h at 600 °C. The furnace temperature was then raised to 800 °C for next 5 h to obtain the homogeneous melt. The ampoules were then quenched in ice water. Thin films were prepared on glass substrates by thermal evaporation of as prepared ZnTe alloy using Hind HIVAC BC-300 in a vacuum  $\sim 4 \times 10^{-6}$  mbar. Prior to deposition, the glass substrates were cleaned by soap solution followed by ultrasonic cleaning and finally with acetone and methanol. Deposition was performed at room temperature with slow rate of 2–3 Å/s to make the composition of thin films close to starting bulk material. The thickness of thin films was monitored using digital thickness monitor (DTM-101) and estimated to be  $\sim 480$  nm using cross-sectional field emission scanning electron microscopy (FE-SEM).

The structural study was performed using PANALYTICAL X'pert-PRO X-ray diffractometer with  $\text{CuK}\alpha$  radiation ( $\lambda = 1.54060\text{\AA}$ ) over the range of 20°–70°. Fourier transform infrared (FT-IR) spectroscopy has been performed using BRUKER-ALPHA in spectral range of 600–4000  $\text{cm}^{-1}$ . For morphological study, FE-SEM images were recorded using Hitachi-SU8010. The elemental composition was obtained from Energy dispersive spectroscopy (EDS) using Bruker X-flash, 6130. A double beam UV–Vis–NIR spectrophotometer (Perkin Elmer Lambda 750) was used to measure normal incidence transmission spectra of thin films in the transmission range 800–3200 nm. Three different as deposited films were annealed in a vacuum of  $\sim 3 \times 10^{-3}$  mbar for an hour, at different temperatures 100, 200 and 300 °C, respectively using a Rotary pump (Model: TLD-75-S). Annealed films were slowly cooled down to avoid thermal shocking. The as deposited, annealed at 100, 200 and 300 °C thin films were labeled as AD, A100, A200 and A300, respectively.

## 3 Results and discussion

Figure 1a shows the X-ray diffraction (XRD) patterns for AD and annealed ZnTe thin films. All the thin films possess cubic ZnTe phase along with some hexagonal Te phase. The diffraction peaks for cubic ZnTe correspond to (111), (220) and (311) planes [ICDD Card no. 01-079-004], whereas hexagonal Te peaks are indexed as (100), (101), (102), (110), (202) and (210) planes [ICDD Card no. 00-003-0506]. The observed values for inter planner spacing ( $d$ ) are in good agreement with standard values. The intensity and sharpness of all ZnTe peaks increases continuously with increasing annealing temperature owing to increase in crystallinity. Kashyout et al. [34] reported increase in sharpness of ZnTe peaks with annealing in argon flux at 375 and 400 °C. Similarly, Mahalingam et al. [28] also observed the increment in sharpness of peaks with annealing in air at 350 °C for 1 h. The intensity of some Te peaks corresponding to

**Fig. 1** **a** X-ray diffraction patterns and **b** size-strain analysis plots for as deposited and annealed ZnTe thin films. (Color figure online)



(100) and (110) planes increases but intensity of peak at (101) decreases on annealing at 100 °C. This trend reverses as annealing temperature is increased up to 200 °C and remains same with further increase in annealing temperature. Increase in sharpness for some Te peaks at (102) and (202), is observed on annealing at 300 °C whereas, peak at (210) diminishes at maximum annealing temperature. The slight shift in peaks was reported by Farooq et al. [35] under vacuum annealing conditions. No such shift is observed in present case of ZnTe thin films. The crystallite size ( $D$ ) and strain ( $\epsilon$ ) were calculated using Hall–Williamson relation [36]:

$$\frac{\beta \cos \theta}{\lambda} = \frac{1}{D} + \frac{\epsilon \sin \theta}{\lambda} \tag{1}$$

where  $\beta$  is the FWHM (full width at half maximum),  $\lambda$  is wavelength of radiation and  $\theta$  is the diffraction angle. Figure 1b represents the plots of  $(\beta \cos \theta)/\lambda$  versus  $(\sin \theta)/\lambda$  for all ZnTe thin films. The crystallite size and strain is determined

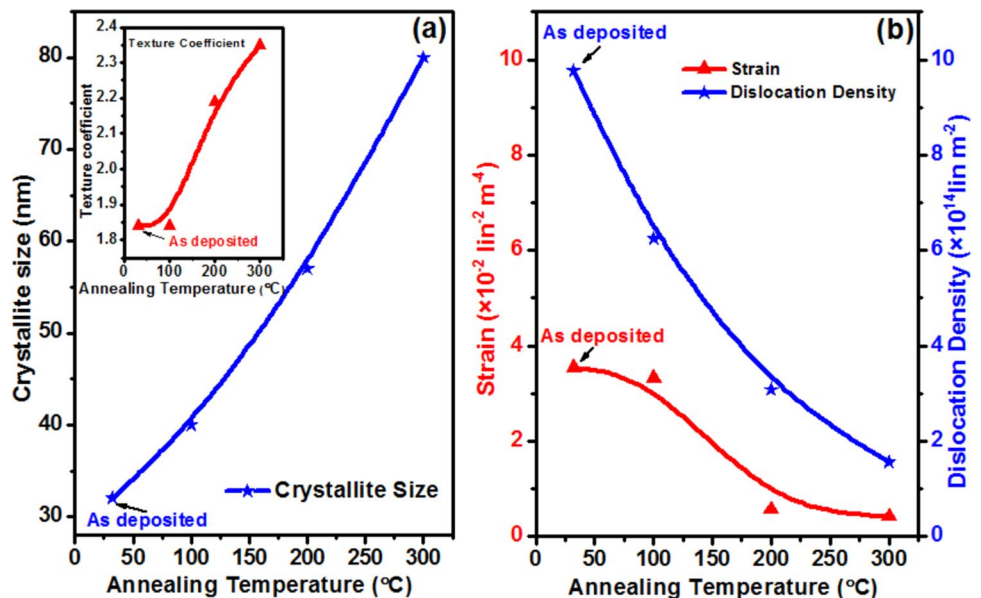
from slopes and intercepts of the plots. The average crystallite size increases with increasing annealing temperature and its value for AD, A100, A200 and A300 films is calculated to be 32, 40, 57 and 80 nm, respectively. The variation of crystallite size with annealing temperature is presented in Fig. 2a.

The micro-strain is observed because of contrast in supplanting of atoms with respect to its original place/station [37]. The micro-strain decreases with increase in annealing temperature, which is due to decrease in lattice defects among the grain boundaries as crystallinity improves upon annealing (Fig. 2b) [20, 38]. The dislocation density ( $\delta$ ), defined as the length of dislocation lines per unit volume of crystal and can be measured by the equation [39]:

$$\delta = \frac{1}{D^2} \tag{2}$$

$\delta$  also decreases with increase in annealing temperature due to decrease in defects in the lattice structure with increase in

**Fig. 2** Variation of **a** crystallite size,  $T_c$  (inset) and **b** strain and dislocation density with annealing temperature for ZnTe thin films



crystallite size (Fig. 2b) [20, 38]. The calculated values of  $\epsilon$  and  $\delta$  have been listed in Table 1.

In order to compare the texture of AD and annealed thin films, texture coefficient ( $T_c$ ) has been calculated by using following equation [40]:

$$T_c(hkl) = \frac{I(hkl)/I_r(hkl)}{n^{-1} \sum I(hkl)/I_r(hkl)} \quad (3)$$

where  $n$  is the number of reflections considered in diffraction pattern;  $I(hkl)$  is the X-ray diffraction intensity obtained from ZnTe thin film samples and  $I_r(hkl)$  is the intensity of reflection from standard diffraction pattern at corresponding angles. It has been reported that  $T_c$  of a direction exceeding unity indicates the preferential orientation in that particular direction [30]. In present case,  $T_c$  values increase for ZnTe phase and decreases for Te phase continuously with increase in annealing temperature (Table 1). This indicates the improvement of ZnTe phase as compared to Te. The increase in texture of (111), (220) and (311) planes can be attributed to improvement in crystallinity of ZnTe thin films [39]. The variation of  $T_c$ , for prominent (111) peak, with annealing temperature is shown in the inset of Fig. 2a.

FT-IR is a characterizing technique used to know about the chemical bonding, vibration and rotation of molecular groups and also the structure and nature of the compounds. The FT-IR spectrum is recorded in 4000–600  $\text{cm}^{-1}$  wave-number range (Fig. 3). The IR transmittance is increased with annealing temperature due to reduction in crystal defects during annealing, which is also reflected in XRD results [37]. The absorption peak around 819.79  $\text{cm}^{-1}$  is attributed to formation of substrate dangling bond (Si–Te) [41]. O–H stretching vibrations are observed at 1594.73 and 3780.86  $\text{cm}^{-1}$ . A peak seen at 2355.39  $\text{cm}^{-1}$  might be due to presence of  $\text{CO}_2$  molecules [42, 43].

FE-SEM images are recorded at 2  $\mu\text{m}$  and 400 nm resolutions to analyze the surface morphology of ZnTe thin films. Figure 4a, b shows that films are found to be uniform and homogeneous. The particles are uniformly distributed covering the surface of glass substrate. There are no crystal defects in thin film due to absence of any pinholes, pitfalls, cracks or voids. Figure 4c presents the cross-sectional FE-SEM image of film, showing the average thickness of  $\sim 480$  nm. EDS spectra is presented in Fig. 4d, the atomic percentage of Te:Zn is measured to be 59.33:40.67. The elemental peaks in EDS spectrum confirm the presence of tellurium

**Table 1** Representation of Crystallite size ( $D$ ), Strain ( $\epsilon$ ), Dislocation density ( $\delta$ ), Dominant peaks, planes (hkl), Texture coefficient ( $T_c$ ) and Optical band gap ( $E_g$ ) for as deposited and annealed ZnTe thin films

Film	$D$ (nm)	$\epsilon$ ( $\text{lin}^{-2} \text{m}^{-4}$ )	$\delta$ ( $\text{lin} \text{m}^{-2}$ )	Dominant peaks ( $^\circ$ )	(hkl)		$T_c$		$E_g$ (eV)
					Te	ZnTe	Te	ZnTe	
AD	32	$3.54 \times 10^{-2}$	$9.77 \times 10^{14}$	23.66	100	–	2.40	–	1.37
				25.94	–	111	–	1.84	
				28.20	101	–	1.66	–	
				41.09	110	–	0.84	–	
				42.47	–	220	–	0.29	
				50.14	–	311	–	0.45	
A100	40	$3.33 \times 10^{-2}$	$6.25 \times 10^{14}$	23.62	100	–	3.12	–	1.06
				25.84	–	111	–	1.84	
				28.19	101	–	0.75	–	
				41.05	110	–	0.88	–	
				42.58	–	220	–	0.47	
				50.18	–	311	–	0.51	
A200	57	$0.57 \times 10^{-2}$	$3.08 \times 10^{14}$	23.71	100	–	1.81	–	0.92
				25.94	–	111	–	2.19	
				28.23	101	–	1.25	–	
				41.08	110	–	0.41	–	
				42.61	–	220	–	0.48	
				50.23	–	311	–	0.68	
A300	80	$0.42 \times 10^{-2}$	$1.56 \times 10^{14}$	23.69	100	–	1.03	–	0.91
				25.92	–	111	–	2.35	
				28.20	101	–	1.61	–	
				41.10	110	–	0.34	–	
				42.55	–	220	–	0.52	
				50.23	–	311	–	0.68	



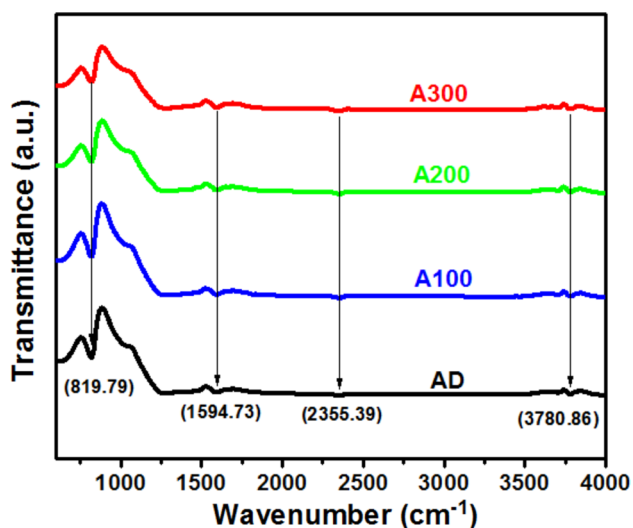


Fig. 3 FT-IR spectra for as deposited and annealed ZnTe thin films

and zinc. The additional peaks seen in spectrum are related to glass substrate.

The transmission spectra of AD and annealed ZnTe thin films (Fig. 5a) show the presence of interference fringes, confirming the formation of uniform and smooth thin films [44]. All the films show good transmittance in NIR region however, transmittance decreases after annealing due to crystal growth and enlarge crystallite size [45]. Low transmittance in visible

region of the spectrum for as-deposited and annealed films reflects good absorption capacity of prepared samples [46]. Aqili et al. [31] also observed decrease in transmittance with annealing in nitrogen ambience. Figure 5a shows that the fundamental absorption edge shifts towards higher wavelengths with increase in annealing temperature due to improvement in crystallinity of thin films. The absorption coefficient ( $\alpha$ ) can be estimated near the band edge, in the region of strong absorption using the equation [47]:

$$\alpha = \frac{1}{t} \ln \left( \frac{1}{T} \right) \quad (4)$$

where  $t$  is the thickness of the film and  $T$  is the transmittance of the film at distinct wavelengths. The behavior of absorption coefficient at different annealing temperatures as a function of photon energy, is shown in Fig. 5b. An increase in  $\alpha$  with annealing is observed.

The absorption coefficient is related to optical band gap by the relation [48]:

$$ahv = A(hv - E_g)^n \quad (5)$$

where  $A$  is constant,  $h\nu$  is photon energy,  $E_g$  is energy band gap, and  $n$  is an integer depending on the nature of electronic transition. For direct allowed transitions,  $n$  has value of 0.5. The optical band gap energy is determined by extrapolating the straight line portion of  $(ahv)^2$  versus incident photon energy plots, as illustrated in Fig. 6. The  $E_g$  for AD, A100, A200 and A300 thin films have been calculated to be 1.37,

Fig. 4 a, b FE-SEM images at 2  $\mu$ m and 400 nm resolutions, c cross-sectional FE-SEM image and d EDS spectrum for ZnTe thin films

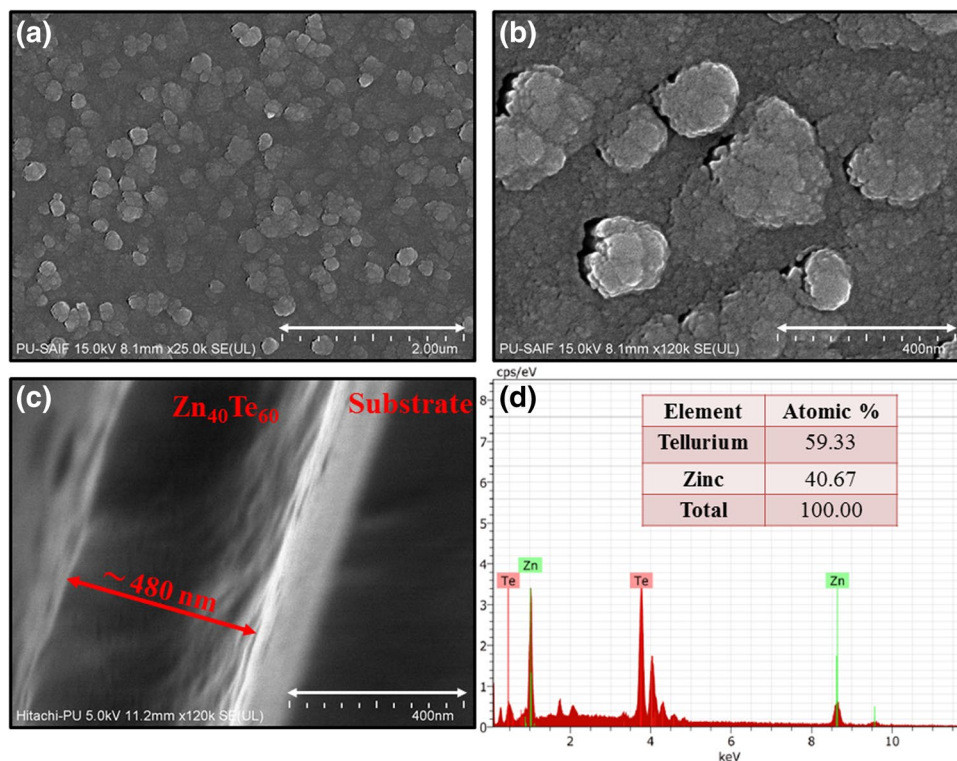


**Fig. 5** **a** Transmission spectra and **b** absorption coefficient for as deposited and annealed ZnTe thin films. (Color figure online)

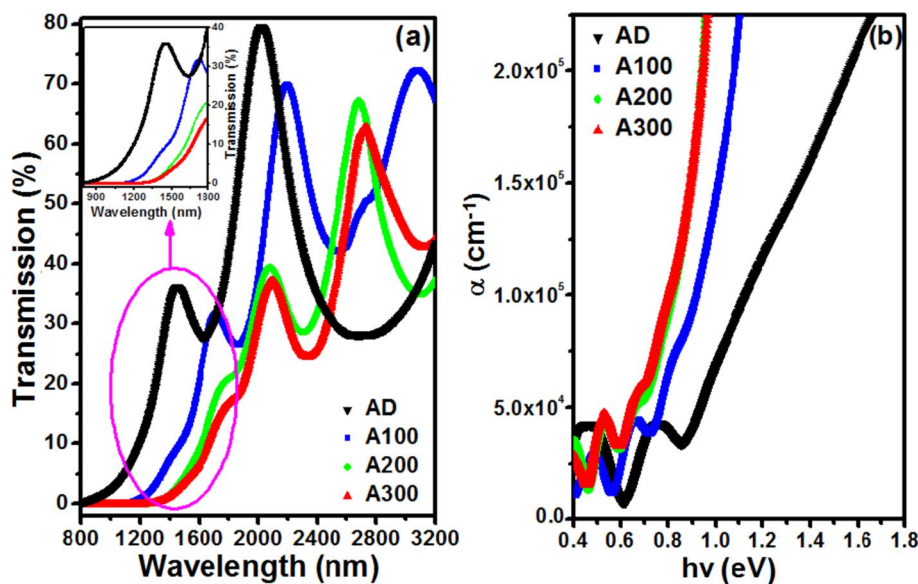
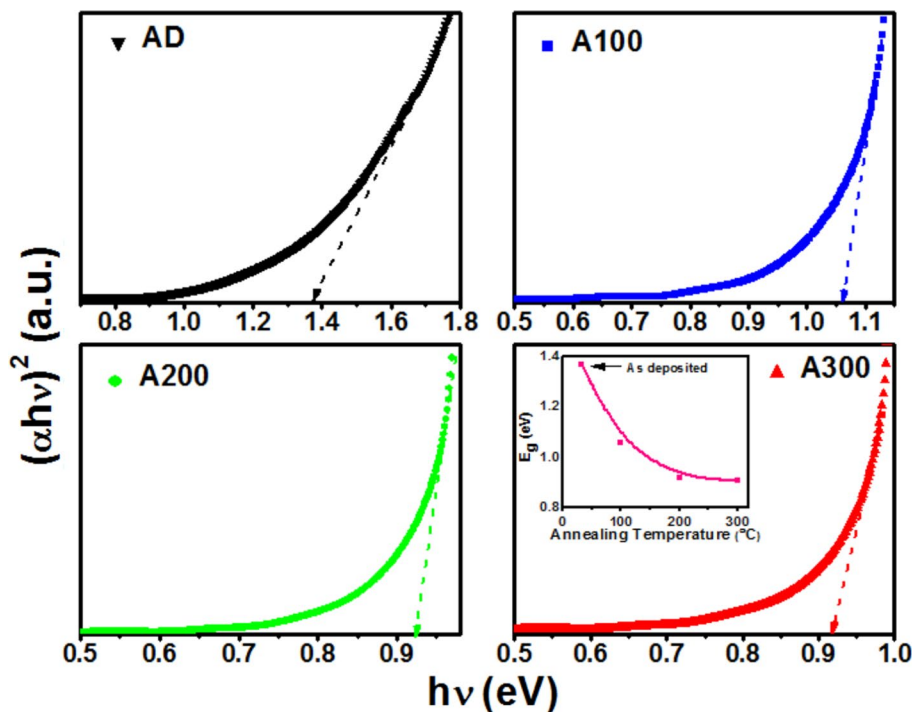


**Fig. 6** The Tauc plots for as deposited and annealed ZnTe thin films, Inset: Variation of band gap with annealing temperature



1.06, 0.92 and 0.91 eV, respectively. The red shift in band gap energy with annealing is attributed to reduction in impurities, improvement in crystallinity and more realignment in orientation [39]. Farooq et al. [35] also found decrease in band gap with annealing ZnTe thin films at 380 °C for 1 h, in vacuum chamber. In general, the optical band gap energy in compound semiconductors can be influenced by disorder at the grain boundaries, dislocation density, stoichiometric deviations, change in preferred orientation and quantum size effect [39, 49, 50]. In the present study, variation in crystallite size and crystallinity is the cause for decrease in band

gap of ZnTe thin films. Variation of optical band gap with annealing temperature is shown in the inset of Fig. 6

### 4 Conclusions

Nanocrystalline ZnTe thin films with thickness of ~ 480 nm are prepared by thermal evaporation technique. These films are annealed in vacuum for 1 h at different temperatures i.e. 100, 200 and 300 °C. To explore the annealing effect on structural and optical properties of prepared samples,

various characterizing techniques such as XRD, FT-IR, FE-SEM and UV–Vis–NIR have been adopted. It is found that as deposited and annealed thin films are nanocrystalline in nature with cubic ZnTe and hexagonal Te mix phase. Crystallinity improves with annealing due to which micro strain and dislocation density decreases. The optical parameters are also dependent on annealing. The red shift in absorption edge on annealing (1.37–0.91 eV) is attributed to improvement in crystallinity owing to realignment in orientation. This indicates that ZnTe thin films are good alternate candidate to toxic Cd-based chalcogenide materials such as CdSe and CdTe in solar cell applications.

**Acknowledgements** Authors (TS) and (AT) are thankful to SERB, New Delhi for the financial support (SR/FTP/PS-081/2012) and (Sanction No. SB/FTP/PS-075/2013 dated 29/05/2014), respectively.

## References

- G. Chen, J. Seo, C. Yang, P.N. Prasad, *Chem. Soc. Rev.* **42**, 8304 (2013)
- J. Huang, Z. Yin, Q. Zheng, *Energy Environ. Sci.* **4**, 3861 (2011)
- D. Sharma, R. Jha, S. Kumar, *Sol. Energy Mater. Sol. Cells* **155**, 294 (2016)
- J.H. Rhee, C.-C. Chung, E.W.-G. Diau, *NPG Asia Mater.* **5**, e68 (2013)
- X. Jin, J. Li, G. Chen, C. Xue, W. Liu, C. Zhu, *Sol. Energy Mater. Sol. Cells* **146**, 16 (2016)
- X. Huang, S. Han, W. Huang, X. Liu, *Chem. Soc. Rev.* **42**, 173 (2013)
- T.K. Todorov, D.M. Bishop, Y.S. Lee, *Sol. Energy Mater. Sol. Cells* (2017) <https://doi.org/10.1016/j.solmat.2017.07.033>
- M. Teena, A.G. Kunjomana, K. Ramesh, R. Venkatesh, N. Naresh, *Sol. Energy Mater. Sol. Cells* **166**, 190 (2017)
- B.I. MacDonald, A. Martucci, S. Rubanov, S.E. Watkins, P. Mulvaney, J.J. Jasieniak, *ACS Nano* **6**, 5995 (2012)
- D.C. Sharma, S. Srivastava, Y.K. Vijay, Y.K. Sharma, *Int. J. Rec. Res. Rev.* **2**, 16 (2012)
- A. Mahmood, R. Rashid, U. Aziz, A. Shah, Z. Ali, Q. Raza, T. Ashraf, *Prog. Nat. Sci.* **25**, 22 (2015)
- K.R. Murali, M. Ziaudeen, N. Jayaprakash, *Solid-State Electron.* **50**, 1692 (2006)
- S. Patra, S.K. Pardhan, *Acta Mater.* **60**, 131 (2012)
- A.K.S. Aqili, A.J. Saleh, Z. Ali, S. Al-Omari, *J. Alloys Compd.* **520**, 83 (2012)
- W. Mahmood, N.A. Shah, *Curr. Appl. Phys.* **14**, 282 (2014)
- C.A. Wolden, A. Abbas, J. Li, D.R. Diercks, D.M. Meysing, T.R. Ohno, J.D. Beach, T.M. Barnes, J.M. Walls, *Sol. Energy Mater. Sol. Cells* **147**, 203 (2016)
- M.A.M. Seyam, *J. Alloys Compd.* **541**, 448 (2012)
- E. Bacaksiz, S. Aksu, N. Ozer, M. Tomakin, A. zelik, *Appl. Surf. Sci.* **256**, 1566 (2009)
- O. Skhouni, A.E. Manouni, M. Mollar, R. Schrebler, B. Mar, *Thin Solid Films* **564**, 195 (2014)
- E.R. Shaaban, I. Kansal, S.H. Mohamed, J.M.F. Ferreira, *Physica B* **404**, 3571 (2009)
- Z. Zhang, J. Li, H. Zhang, X. Pan, E. Xie, *J. Alloys Compd.* **549**, 88 (2013)
- O.I. Olusola, M.L. Madugu, N.A. Abdul-Manaf, I.M. Dharmadasa, *Curr. Appl. Phys.* **16**, 120 (2016)
- H. Ko, S. Park, S. An, C. Lee, *J. Alloys Compd.* **580**, 316 (2013)
- T. Nakasua, W. Suna, M. Kobayashia, T. Asahi, *J. Cryst. Growth* **16**, 120 (2016)
- G. Lastra, P.A. Luque, M.A. Quevedo-Lopez, A. Olivias, *Mater. Lett.* **126**, 271 (2014)
- T. Potloga, D. Duca, M. Dobromir, *Appl. Surf. Sci.* **352**, 33 (2015)
- A.A. Ibrahim, N.Z. El-Sayed, M.A. Kaid, A. Ashour, *Vacuum* **75**, 189 (2004)
- T. Mahalingam, V.S. John, S. Rajendran, G. Ravi, P.J. Sebastian, *Surf. Coat. Technol.* **155**, 245 (2002)
- C.S.A. Raj, F.P. Xavier, *Arch. Appl. Sci. Res.* **5**, 167 (2013)
- S. Shanmugan, S. Balaji, K. Ramanathan, *Optoelectron. Adv. Mater.-Rapid Commun.* **3**, 468 (2009)
- A.K.S. Aqili, Z. Ali, A. Maqsood, *J. Cryst. Growth* **317**, 47 (2011)
- M.I. Hossain, M. Kamruzzaman, A.B.M.O. Islam, *J. Mater. Sci.* **26**, 1756 (2015)
- H. Singh, P. Singh, A. Thakur, T. Singh, J. Sharma, *Mater. Sci. Semicond. Process.* **75**, 276 (2018)
- A.B. Kashyout, A.S. Aric, P.L. Antonucci, F.A. Mohamed, V. Antonucci, *Mater. Chem. Phys.* **51**, 130 (1997)
- M.U. Farooq, M. Khan, A. Faraz, A. Maqsood, W. Ahmad, L. Li, *Mater. Technol.* **29**, 29 (2014)
- J. Sharma, R. Singh, H. Singh, T. Singh, P. Singh, A. Thakur, S.K. Tripathi, *J. Alloys Compd.* **724**, 62 (2017)
- S. Chander, M.S. Dhaka, *Thin Solid Films* **638**, 179 (2017)
- M.A. Abdel-Rahim, M.M. Hafiz, A.Z. Mahmoud, *Solid State Sci.* **48**, 125 (2015)
- S. Chander, M.S. Dhaka, *Physica E Low dimens. Syst. Nanostruct.* **80**, 62 (2016)
- D. Shikha, V. Mehta, S.C. Sood, J. Sharma, *J. Mater. Sci.* **26**, 4902 (2015)
- Q. Gul, M. Zakria, T.M. Khan, A. Mahmood, A. Iqbal, *Mater. Sci. Semicond. Process.* **19**, 17 (2014)
- W. Mahmood, N.A. Shah, S. Akram, U. Mehboob, U.S. Malik, M.U. Sharaf, *Chalcogenide Lett.* **11**, 461 (2014)
- B. Ghosh, D. Ghosh, S. Hussain, R. Bhar, A.K. Pal, *J. Alloys Compd.* **541**, 104 (2012)
- A.R. Balu, V.S. Nagarethinama, A. Thayumanavana, K.R. Murali, C. Sanjeeviraja, M. Jayachandran, *J. Alloys Compd.* **502**, 434 (2010)
- S.J. Ikhmayies, *Int. J. Hydrog. Energy* **41**, 12626 (2016)
- A. Hussain, R. Ahmed, N. Ali, N.M. Abdel-Salam, K.B. Derman, Y.Q. Fu, *Surf. Coat. Technol.* **320**, 404 (2017)
- J. Sharma, S.K. Tripathi, *Physica B* **406**, 1757 (2011)
- J.I. Pankove, *Optical Processes in Semiconductors* (Prentice-Hall, Englewood Cliffs, New Jersey, 1971)
- E. Bacaksiz, B.M. Bsol, M. Altunbas, V. Novruzov, E. Yanmaz, S. Nezir, *Thin Solid Films* **515**, 3079 (2006)
- S.S. Lin, J.L. Huang, *Surf. Coat. Technol.* **185**, 222 (2004)